RILEM Technical Letters (2024) 9: 106-116
https://doi.org/10.21809/rilemtechlett.2024.204

Quantifying the early-age viscoelastic properties of alkali activated slag concrete using repeated minutes-long creep tests

Zhenming Li[1,2,+,a,*] Jiawei Xu[1,2,a], Liang Minfei[3], Guang Ye[3], Jinping Ou[1,2]

[1]School of Civil and Environmental Engineering, Harbin Institute of Technology, China
[2]Guangdong Provincial Key Laboratory of Intelligent and Resilient Structures for Civil Engineering, Harbin Institute of Technology, China
[3]Department of Materials, Mechanics, Management & Design, Faculty of Civil Engineering and Geoscience, Delft University of Technology, the Netherlands
+Zhenming Li was invited for submission of this letter as an awardee of the Gustavo Colonnetti Medal granted by RILEM in 2024
[a]These authors contributed to this work equally

Received: 18 November 2024 / Accepted: 18 February 2025 / Published online: 26 February 2025

Abstract

The early-age viscoelasticity of alkali-activated slag concrete (AASC) is critical for its early-age cracking proneness and long-term performance, particularly regarding creep and internal stress development. This study employs an innovative approach to quantify the early-age viscoelastic behavior of AASC, utilizing a Temperature Stress Testing Machine to conduct compressive, repeated and minutes-long creep tests, covering the curing age from 6 h till 28 days. This study is based on the linear theory of viscoelasticity and the Boltzmann superposition principle. A double power law function is employed to model creep and to further predict the internal stress of restrained AASC. It is demonstrated that the double power law function accurately captures the short-term creep of AASC, enabling reliable predictions of early-age stress accumulation and relaxation. Overall, this study highlights the pronounced viscoelasticity of AASC and the effectiveness of the experimental and modelling approaches used to quantify it.

Keywords: Alkali-activated slag; Viscoelasticity; Creep; Relaxation; Modelling.

1 Introduction

Alkali-activated slag (AAS) has garnered significant attention from both academia and industry as a promising low-carbon alternative to traditional Portland cement (PC)[1,2]. As environmental concerns intensify, the construction sector is increasingly focused on sustainable practices. The utilization of industrial by-products has become a key strategy for reducing the carbon emissions associated with construction materials [3]. Beyond the environmental benefits, alkali-activated slag concrete (AASC) exhibits excellent mechanical properties and durability [4–7]. Nonetheless, the widespread adoption of AAS in the construction industry has been limited by several performance-related challenges, notably autogenous shrinkage and early-age cracking [8–11].

While shrinkage and cracking of concrete are always mentioned together as cause and effect, the quantitative relationship between them remains unclear [12], especially for AASC, which exhibits significant time-dependent behavior [13,14]. Creep, a time-dependent deformation under sustained stress, plays a significant role in the overall shrinkage of concrete. It has been reported that AAS shows much larger creep compared to PC, particularly in the early stages [15,16]. On the other hand, stress relaxation can reduce internal stress under restrained conditions, potentially helping to alleviate some of the stress caused by shrinkage and lowering cracking risk. However, in some other scenarios, such as prestressed concrete, relaxation has a detrimental effect since it can decrease the prestress level, contributing to long-term deflection and compromised structural stability [17,18]. The bonding between concrete and rebar is also affected by the local relaxation as the friction is determined by the compressive stress between them. Creep and relaxation are like two sides of one coin – viscoelasticity. A clear understanding of the viscoelastic response of AASC is essential not only to estimate its early-age deformation and cracking proneness [19], but also to evaluate the long-term performance of reinforced concrete structures [20,21].

Despite the recognized importance of viscoelastic properties, most current predictive models for AASC focus on its hardened state, often neglecting the critical early-age periods when the material undergoes rapid changes in its chemical

*Corresponding author: Zhenming Li, E-mail: zhenmingLi@hit.edu.cn

and mechanical properties [21,22]. Traditional creep models [23] developed for PC-based concrete may not fully capture the time-dependent behavior of AASC, especially during the early stages of hydration. Consequently, specialized experimental methods and models are necessary to address the early-age viscoelastic characteristics of AASC [19].

A few studies have investigated the early-stage creep properties in cementitious materials at different scales [19,24–28], but experimental results on the relaxation phenomenon of alkali-activated concrete at early ages are scarce [29]. This shortage makes it difficult to accurately predict deformation and internal stress under restrained conditions, leaving researchers reliant on empirical models, such as the model adapted by Li et al. [30] based on studies of OPC, as indicated in the thesis of van Breugel [31]. Testing the early-stage viscoelastic behavior of alkali-activated concrete can enhance comprehension of its time-dependent properties and provide valuable input for the early-age stress modelling efforts.

Therefore, this study aims to quantify the early-age viscoelastic properties of AASC through a series of minutes-long creep tests conducted using a Temperature Stress Testing Machine (TSTM). The experimental method employed in this study closely resembles the one proposed by Delsaute et al. [19,32,33] for PC concrete. By employing a double power law function and the Boltzmann superposition principle, this research seeks to model the creep behavior of AASC. The creep testing data serves as input for early-age stress modelling to predict the internal stress evolution of the AASC under restrained condition during the early stages of hardening. These findings will provide a better understanding of the viscoelastic characteristics of AASC.

2 Materials and mixtures

2.1 Raw materials

The primary raw material used in this study was ground granulated blast furnace slag (hereafter referred to as slag), which served as the precursor for the AASC. The slag was supplied by Ecocem Benelux BV, and its chemical composition was analyzed using X-ray fluorescence (XRF), as shown in Table 1. The slag particles had a size distribution ranging from 0.1 to 50 μm, with a median particle diameter (d50) of 18.3 μm, and a density of 2.89 g/cm³.

The alkaline activator was prepared by combining anhydrous sodium hydroxide pellets with deionized water and a commercial sodium silicate solution (Na_2SiO_3), sourced from Brenntag. The Na_2SiO_3 solution contained 27.5 wt% SiO_2 and 8.25 wt% Na_2O. The mixture was formulated to achieve an activator modulus (MS ratio, SiO_2/Na_2O) of 1.5. For each 100 g of activator, the composition consisted of 13.8 g SiO_2, 9.4 g Na_2O, and 76.8 g water. This yielded a water-to-solid ratio of 0.344 for the paste.

2.2 Mixture proportions

The mixture proportion of AASC is provided in Table 2. The resulting AASC mix was subjected to experimental testing, with a specific focus on its early-age viscoelastic properties.

Table 1. Chemical compositions of slag.

Raw materials	Oxide (wt. %)								
	CaO	Al_2O_3	SiO_2	MgO	Fe_2O_3	SO_3	K_2O	TiO_2	Other
Slag	40.50	13.25	31.77	9.27	0.52	1.49	0.34	0.97	1.89

Table 2. Mixture composition of AASC (kg/m³).

Mixture	Slag	Activator	Aggregate [0–4 mm]	Aggregate [4–8 mm]	Aggregate [8–16 mm]	Volume fraction of aggregate
AASC	400	200	789	440	525	0.67

3 Experimental

In this study, repeated creep minutes-long creep tests were conducted by a TSTM. The elastic modulus (reported in a previous study [34]) and creep compliance (derived from this study) of AASC are used as inputs for modelling the relaxation modulus and internal stress, which will be detailed in Section 4.

3.1 Setup

The TSTM was designed specifically to monitor temperature deformation and the corresponding restrained stress it generates. The redesigned TSTM at Technische Universiteit Delft [35] was expanded to encompass additional applications, including creep and relaxation tests. A complete description of the TSTM can be found in Ref. [12]. The TSTM is capable of simultaneously accounting for various functions, such as temperature control, strain monitoring, and stress applying, thereby facilitating the acquisition of creep data for early-age concrete.

The specimen used for testing had a dog-bone shape with a prismatic testing section in the center, measuring 750 × 150 × 100 mm³ (Figure 1). The specimen was cast in wooden molds with low thermal conductivity to ensure minimal heat exchange during the tests. To minimize friction and shear at the mold-specimen interface, a thin layer of Vaseline was applied to the inner mold surface which was made of thin steel plates, followed by a plastic film. This treatment minimized stress heterogeneity and ensured that the measured stress reflected the intrinsic behavior of concrete. Once cast, the specimen was sealed to prevent moisture loss and placed under restrained conditions for stress measurement. During hardening, the temperature changes at the head sections of the AASC differed slightly from those in the middle, resulting in varying thermal deformations. In

contrast, the temperature within the prismatic section of interest remained largely uniform. The temperature of concrete was measured using thermocouples located in the center line of the specimen in an Autogenous Deformation Testing Machine. Measurements were recorded every minute after the concrete was cast. Further details on the temperature measurement process can be found in [34]. Actually, the steel claws gripping the concrete heads had higher thermal conductivity than the foam mold in the middle, leading to slightly faster heat loss at the "head" sections. But the volume of the “head” parts was also larger. Eventually, the middle part exhibited a slightly higher temperature the sides. This might be a potential source of error in the thermal deformation calculation.

The TSTM applied precise compressive and tensile forces through a horizontal steel frame, with stress measurements starting 6 h after casting and continuing for 28 days. During the creep testing, the force and deformation measurements were recorded per 0.1 s, while measurements were taken at one-second intervals during other periods. The TSTM has a displacement measurement accuracy of 1 µm and a force accuracy of 0.05 kN. This experimental setup enabled accurate capture of early-age viscoelastic behavior, particularly the time-dependent deformation associated with creep and relaxation processes.

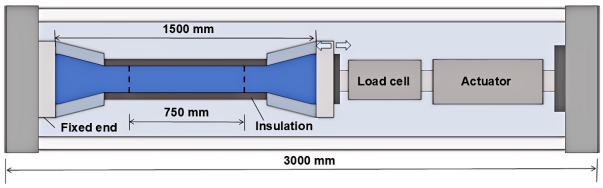

Figure 1. Temperature Stress Testing Machine (TSTM).

3.2 Repeated minutes-long creep tests

Creep of concrete is generally categorized into short-term and long-term phases [36]. Although conventional testing requires extended loading durations, Delsaute et al. [19,28,33,37] have demonstrated that the repeated minutes-long creep tests can effectively capture essential viscoelastic properties during various stages of early-age hardening, offering valuable insights into its behavior.

The repeated minutes-long creep testing protocol involved applying a controlled compressive load to the specimen for a short duration of 6 minutes. The force was applied to generate a stress approximately 15% of the compressive strength, which was estimated based on the strength of AASC cured under isothermal conditions [34]. The stress magnitude of around 15% was chosen to ensure that the material remained within the elastic range and was not damaged during the test cycles [34,38]. The load application was nearly instantaneous, applied in under 1 s, to minimize the effects of loading time on time-dependent behavior. This approach allows us to isolate and analyze the subsequent creep deformation.

During loading, the force was maintained at a high level of accuracy (the target force actually fluctuated with an accuracy of about ±0.0015 kN), avoiding overshoots that could destabilize the system. The unloading process was carried out at a fixed rate of 1 kN/s to facilitate the calculation of the elastic modulus. A minimal compressive load of 0.3 kN was maintained between cycles to ensure continuous contact and stability. Force and deformation data were recorded every 0.1 s during loading and unloading.

To illustrate the loading and unloading behavior, an example of a load cycle is presented, showing the rapid initial loading phase and the slower controlled unloading phase, as shown in Figure 2. The loading-unloading cycle was applied every 2 h in the first 14 h of curing, decreasing in frequency thereafter. We continued these repeated minutes-long creep tests from 6 hours up to 28 days.

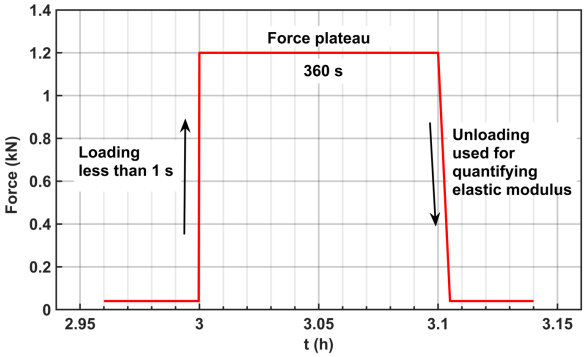

Figure 2. Loading protocol during the first few minutes-long creep tests.

In this study, the uniaxial stress history $\sigma(t)$ in the loading direction is quantified as follows:

$$\sigma(t) = \frac{F(t)}{A} \quad (1)$$

where $F(t)$ is the prescribed force history and $A = 100(mm)\text{x}150(mm) = 15000mm^2$ is the cross-sectional area of the specimen. The uniaxial strain history $\varepsilon(t)$ was measured based on the average of the length changes of the 4 LVDT measurements as follows:

$$\varepsilon(t) = \frac{1}{4}\sum_{i=1}^{4} \Delta S_i(t)\text{x}\frac{1}{750\ mm} \quad (2)$$

where ΔS_i represents 4 LVDT measurements and 750 mm is the measurement length.

3.3 Evolution of elastic modulus and temperature

In this study, the elastic modulus is determined using the displacement and force data recorded during each unloading phase of the repeated creep tests. Figure 3 presents the evolution of the elastic modulus and temperature, clearly illustrating their correlation. The results show the significant increase in elastic modulus throughout 28 days, reflecting ongoing chemical reactions and the resulting increase in stiffness. The increase in the modulus during the first 48 h is fast and corresponds to the acceleration and deceleration period of the concrete, when its temperature remains higher than 23 °C. Subsequently, the growth rate of modulus slows as heat release from the reaction also stabilizes. It is evident

that the temperature drops over the first 7 days and then plateaus, mirroring the evolution of the elastic modulus.

To capture this evolution as an input for modelling in the following section, the elastic modulus is fitted using an empirical function based on that given in the American Concrete Institute (ACI) code [39]. The fitted function is expressed as:

$$E(t') = \frac{30.88t'}{78.68 + 9.404 \text{ x } 10^{-2}t'} \quad (3)$$

where $E(t')$ represents the elastic modulus in MPa and t' is the time in seconds. A previous study [40] shows that different elastic modulus models have minimal impact on the overall model predictions. While deviations were observed during Days 2-4 due to the distinct chemical kinetics of AASC, the results shown in Figure 3 indicate that the fitted function provides an acceptable estimation of the modulus over time, which is then incorporated into the viscoelastic modelling of AASC.

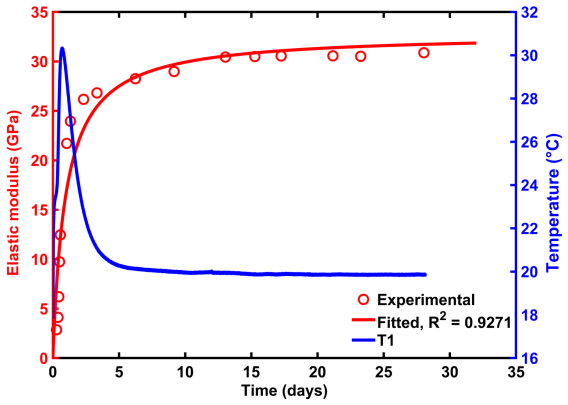

Figure 3. Evolution of elastic modulus (red) and temperature (blue, named T1) of the AASC. The data of temperature is from Ref. [34].

3.4 Calculation of creep/relaxation from measurements

The assessment of viscoelastic properties involves two primary parameters. The first is the elastic modulus, which measures resilience and stiffness during elastic deformation and can be obtained from the force-displacement curve in a loading or unloading test. The second parameter is either creep compliance, which quantifies time-dependent deformation (creep), or relaxation modulus, which evaluates how stress evolves over time. To evaluate these parameters, deformation tests are used to measure creep compliance, while stress relaxation tests are employed to assess the relaxation modulus. During the repeated, minutes-long creep tests, the material undergoes alternating phases of creep and relaxation. In this section, we describe the definitions of creep compliance and relaxation modulus in detail. The obtained creep compliance is used as an essential input for modelling.

3.4.1 Creep compliance

In the minutes-long creep testing, the deformation history of the specimen $\varepsilon(t)$ was measured continuously. Free deformations (including autogenous and thermal deformation), were quantified using an Autogenous Deformation Testing Machine (ADTM) in a previous study [34]. By measuring the total deformation and subtracting the instantaneous and free deformations, the creep deformation is the difference between $\varepsilon(t)$ and $\varepsilon(t')$: $\varepsilon(t,t') = \varepsilon(t) - \varepsilon(t')$. Creep compliance $J(t,t')$ describes the strain response at time t induced by a constant unit stress from time t'. For each loading cycle, the creep compliance $J(t,t')$ can be obtained by the following expression:

$$J(t,t') = \frac{\varepsilon(t,t')}{\sigma(t')} \quad (4)$$

where $\sigma(t')$ is the stress at loading. Creep coefficient, another expression of viscoelasticity, is related to the creep compliance $J(t,t')$, as expressed as:

$$J(t,t') = \frac{1+\varphi(t,t')}{E(t')} \quad (5)$$

where $E(t')$ is the elastic modulus and $\varphi(t,t')$ is the creep coefficient, defined as the ratio between creep strain and elastic strain.

Figure 4 shows the creep compliance curves for the selected time points, highlighting the evolution of the viscoelastic response during hardening. The time-dependent creep compliance of AASC was examined over a period ranging from 1 h to 168 h. Actually, later-age tests were also conducted, but the results are not shown here for the purpose of simplicity. For instance, the creep coefficient at 28 days (included in Appendix A) is compared with Kostiuchenko [41]. The results in Figure 4 show that aging has a significant impact on the magnitude of basic creep compliance, with loading applied at earlier ages yielding higher basic creep compliance.

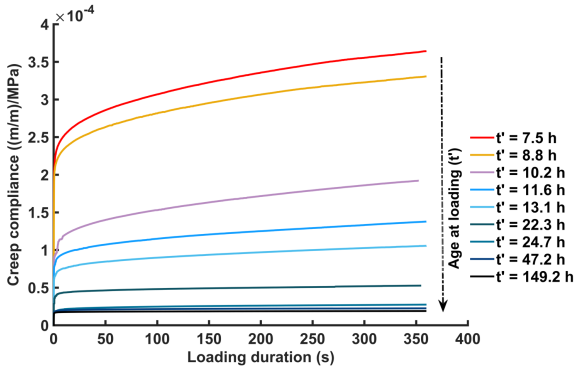

Figure 4. Creep compliance from repeated minutes-long creep tests at early age.

3.4.2 Relaxation modulus

The relaxation modulus defines the stress response corresponding to a unit strain applied. In the general theory of relaxation experiments with TSTM from the literature [32] and assumed that the strain at the end of each 6-minute creep test represents the strain over the entire duration, relaxation modulus $R(t,t')$ can be obtained by the following expression:

$$R(t,t') = \frac{\sigma(t,t')}{\varepsilon(t')} \quad (6)$$

where t' is the end time of the loading cycle; $\varepsilon(t')$is the constant strain at t'; $\sigma(t,t')$ is the stress difference

between $\sigma(t)$ and $\sigma(t')$: $\sigma(t,t') = \sigma(t) - \sigma(t')$. Although theoretically the constant strain $\varepsilon(t')$ was applied for a finite period of time in the experiment, it is also considered to be applied instantaneously.

However, stress relaxation testing is more complex, not only requiring a measurement of strain but also an active adjustment of the load to maintain a constant strain. In contrast, creep testing is simpler, as it involves keeping the load constant and measuring the strain. Consequently, most studies use creep testing to quantify viscoelastic properties. For early-age concrete simulations, it is significant to convert the measured creep compliance into a relaxation modulus [42].

4 Modelling

Creep prediction models can be categorized into two primary types: empirical models and numerical models. Empirical models are generally derived from comprehensive statistical analysis of macroscale test data, while numerical models are grounded in micromechanical principles. By incorporating time-dependent viscoelastic properties, such as aging creep and elastic modulus, as key input parameters, the model can effectively perform accurate internal stress analysis. In this section, the double power law function is utilized to simulate the creep compliance of AASC. Then, the relaxation modulus is obtained through creep-relaxation conversion and used as an input to simulate the evolution of internal stress. The discrepancies between the predicted and measured results are analyzed.

4.1 Theory

In this section, the Boltzmann superposition principle and the evolution of internal stress are described. During the hardening process of cementitious materials, various phenomena including autogenous shrinkage, thermal deformation, and expansion-induced deformation occur. The TSTM can accurately impose reverse deformation to counteract these deformations and achieve a fully restrained state. Concrete in this condition generates internal stress. Assuming the concrete behaves in a linearly elastic manner, the early-age stress for each time step can be represented as follows:

$$\Delta\sigma(t') = E(t')\Delta\varepsilon(t') \tag{7}$$

where t' stands for the moment when the load is initially applied. The evaluation of the specified creep experiments is conducted within the context of the linear theory of viscoelasticity, employing Boltzmann's superposition principle to correlate the prescribed stress history $\sigma(t)$ with the measured strain evolutions $\varepsilon(t)$. The total early-age stress can be expressed as:

$$\sigma(t) = \int_0^t E(t')d\varepsilon(t') \tag{8}$$

By replacing the elastic modulus with the relaxation modulus, thus, the following integral equation is obtained as:

$$\sigma(t) = \int_0^t R(t,t')\frac{\partial\varepsilon}{\partial t'}dt' \tag{9}$$

where R denotes the relaxation modulus; $\frac{\partial\varepsilon}{\partial t'}$ is the time-derivative of the retrained strain history $\varepsilon(t)$; t is the moment of interest. The integration of Equation (9) can be approximated using the midpoint rule:

$$\sigma(t) = \sum_{t'=0}^{t'=t} R\left(t,t' + \frac{1}{2}\Delta t'\right)\mathrm{x}\Delta\varepsilon(t') \tag{10}$$

By incorporating the deformation rate $\Delta\varepsilon$ and the viscoelastic relaxation modulus $R(t,t')$, it is possible to accurately simulate the evolution of early-age stress. The deformation rate $\Delta\varepsilon$ can easily obtained from the test. With a linear viscoelastic constitutive relationship, creep compliance $J(t,t')$ and relaxation modulus $R(t,t')$ are not completely independent. In general, the strain history at t can be expressed as:

$$\varepsilon(t) = J(t,t')\sigma(t') + \int_{\hat{t}=t'}^{\hat{t}=t} J(t,\hat{t})\frac{d\sigma(\hat{t})}{d\hat{t}}d\hat{t} \tag{11}$$

where $\hat{t}$ is the time step. According to the definition of relaxation modulus and the boundary of a relaxation test, Equation (11) can be expressed as below [43]:

$$J(t,t')R(t',t') + \int_{\hat{t}=t'}^{\hat{t}=t} J(t,\hat{t})\frac{dR(t',\hat{t})}{d\hat{t}}d\hat{t} = 1 \tag{12}$$

where R is the relaxation modulus. Therefore, the creep compliance $J(t,t')$ and the relaxation modulus $R(t,t')$ can be converted into each other through Equation (12).

4.2 Double power law model

Over the past few decades, predictive creep models developed have primarily focused on the viscoelastic properties of concrete, frequently neglecting its hardening characteristics. The double power law model is an approach to account for the aging effect in concrete by capturing the evolution of elastic modulus [23,44,45]. Applying the double power law to early-age crack prediction and stress simulation in concrete has shown promising results [43,46,47]. In this study, the double power law [23], as presented in Equation (13), is used specifically for the early-age creep in AASC. Notably, for long-term creep, a logarithmic function would be more appropriate [43,48].

$$J(t,t') = \frac{1}{E(t')} + a\cdot\left(\frac{1}{t'}\right)^b\cdot(t-t')^c \tag{13}$$

where $J(t,t')$ is the creep compliance function; $E(t')$ is the elastic modulus at loading time; a, b, and c are creep model fitting parameters that are obtained from tests; t is the time of interest; t' is the concrete age (the time when creep testing load is applied); $t-t'$ is the loading time.

Before fitting Equation (13), the experimentally obtained data is first evaluated using a non-aging power function [43] to validate its accuracy, expressed as

$$J(t) = a\cdot t^r \tag{14}$$

where a and r are the fitting parameters. The accuracy of the model is further validated by calculating the root mean square error (RMSE) between the fitted and experimental creep compliance values. An RMSE value approaching zero

indicates that the model prediction closely aligns with the experimental data. The formula for RMSE is as follows:

$$RMSE = \sqrt{\frac{\sum_N (Y_c - Y_r)^2}{N}} \quad (15)$$

where N is the amount of the considered points; Y_c is the fitted value and Y_r is the experimental value.

According to Equation (14), the creep compliances at the selected ages are individually normalized with respect to the sustained load level to confirm the validity, as depicted in Figure 5. The results show that the creep compliance function $J(t,t')$ show a strong correlation with the predicted model curves, as indicated by the close alignment between the experimental data (blue lines in Figure 5) and the model predictions (red lines in Figure 5). According to Equation (15), The maximum RMSE value of 4.84 x 10^{-6} which is close to zero (less than 1E-05), indicates that the model effectively captures the creep behavior of AASC within the early-age period. Additionally, the model predictions are highly accurate, with a maximum relative error of 1.8% (calculated as the RMSE divided by the mean measured compliance value), and their robustness is further supported by the prediction band of the 95% confidence interval, depicted as the light purple area in Figure 5.

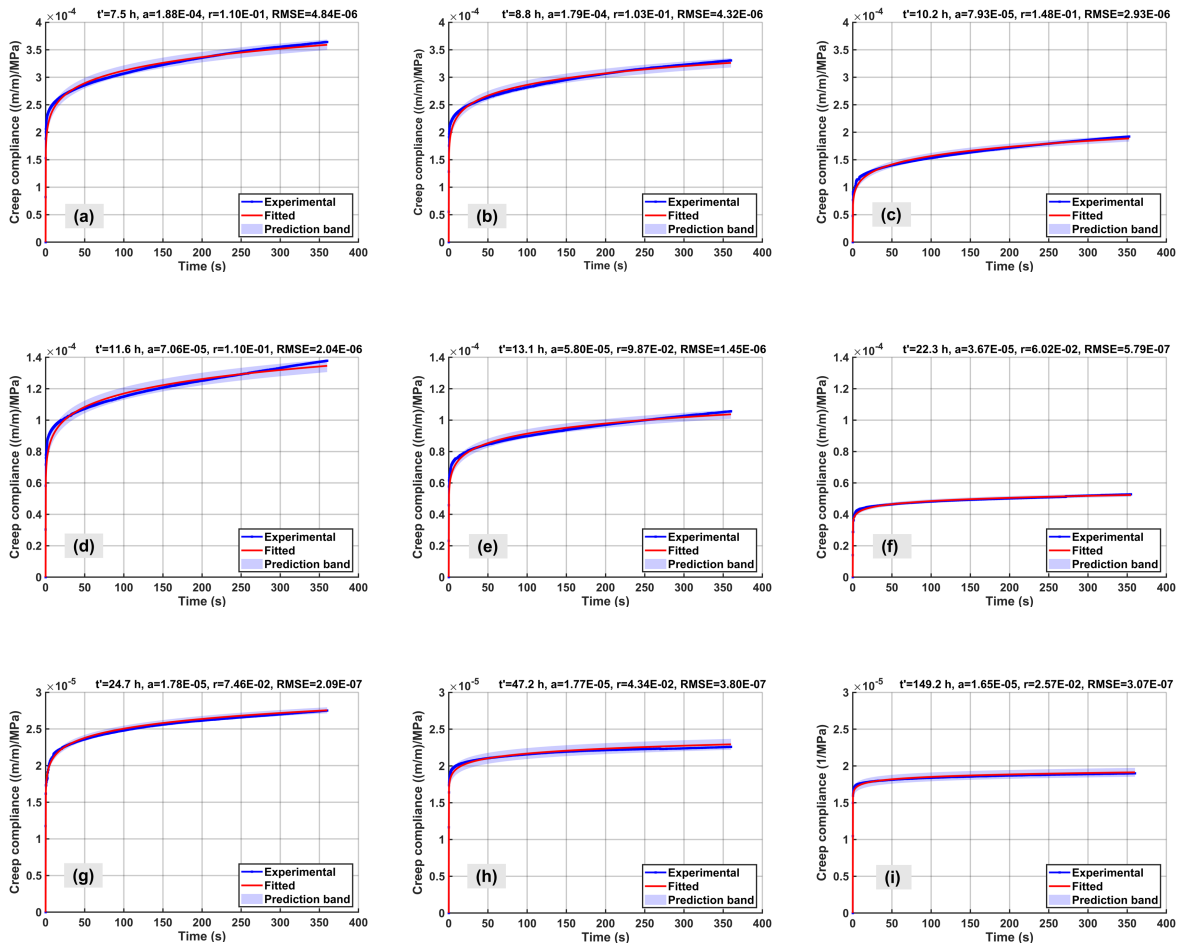

Figure 5. Testing results of creep compliance (the blue solid lines refer to measurements obtained from testing, the red solid lines refer to predicted model by a non-aging power function and the light purple area represents the 95% confidence interval of creep compliance.): (a) t'=7.5 h; (b) t'=8.8 h; (c) t'=10.2 h; (d) t'=11.6 h; (e) t'=13.1 h; (f) t'=22.3 h; (g) t'=24.7 h; (h) t'=47.2 h; (i) t'=149.2 h

Finally, in accordance with Equation (4), all the obtained basic data were utilized to fit the double power law function. The calculated creep compliance function is presented as follows:

$$J(t,t') = \frac{1}{E(t')} + 40.95\text{x}\left(\frac{1}{t'}\right)^{1.523}(t-t')^{0.374} \quad (16)$$

where $E(t')$ is obtained from Equation (3); t and t' are in seconds; creep compliance function $J(t,t')$ is in $(m/m)/MPa$. The calculated parameters reveal the influence of composition, aging time and loading duration on creep behavior [43]. Figure 6 compares the calculated and experimental creep compliance results. To more clearly illustrate long-term trends, the loading duration is extended to 200 h, although the experimental data (solid line in Figure 6) only spans up to 360 seconds. This function provides a satisfactory fit, with an R^2 value of 0.84, indicating a moderate yet reliable alignment with the early-age

viscoelastic properties. It should be noted that the model extrapolation into longer timescales is based on early-age creep data from minutes-long tests. While this approach has proven effective for early-age predictions, caution is needed when applying it to long-term predictions. Experimental validation of these predictions over extended periods will be critical.

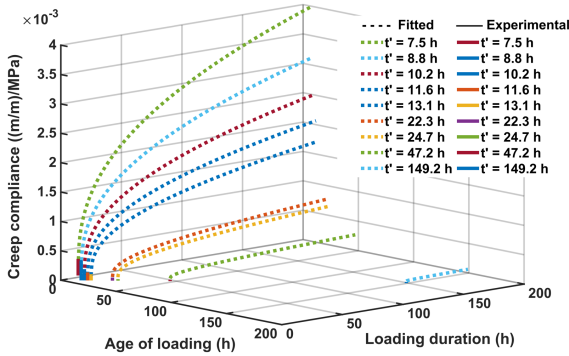

Figure 6. Evolution of creep compliances obtained from repeated minutes-long creep tests and modelling. Note that each dashed line begins with a short segment of experimental data, which appears small due to differences in the time scale.

According to Equations (3), (5) and (16), the creep coefficient $\varphi(t,t')$ calculated in this study can be expressed as:

$$\begin{aligned}\varphi(t,t') &= 40.95\text{x}E(t')\cdot\left(\frac{1}{t'}\right)^{1.523}\cdot(t-t')^{0.374}\\ &= 40.95\text{x}\left(30.88\text{x}\frac{t'}{78.68+9.404\text{x}10^{-2}t'}\right)\cdot\left(\frac{1}{t'}\right)^{1.523}\\ &\cdot(t-t')^{0.374}\\ &= \frac{1264.536}{78.68+9.404\text{x}10^{-2}t'}t'^{-0.523}(t-t')^{0.374}\end{aligned} \quad (17)$$

where t and t' are in seconds. It is noteworthy that the results for the creep coefficient φ are relatively similar to an empirical equation reported in Ref. [34].

Previous studies have reported that the evolution of creep compliance for the short terms creep tests can be expressed by a power law function:

$$J(t,t') = \alpha\left(\frac{t-t'}{t_1}\right)^{\beta} \quad (18)$$

where t_1 is the time unit, i.e. 1 s. It is commonly observed that the power-law exponent β in concrete samples exhibits a narrow variation, ranging from 0.30 to 0.45 [49–51]. More interestingly, a range of values between 0.20 and 0.40 has also been observed in cement paste samples [37,45,52–54]. Although the predictive creep model used in this study is based on a double power law, the power-law exponent β (0.374) remains exactly within this range, underscoring the reliability of the results. It is noteworthy that there is a significant lack of literature focused on simulating the viscoelastic properties of AASC. Comparing the model data obtained from creep experiments with OPC concrete can provide valuable support for the findings of this study.

4.3 Creep-relaxation conversion

According to Equations (9) and (10), the internal stress can be obtained directly, but requires the conversion from creep compliance to relaxation modulus. In this study, two representative methods for conversion are employed: numerical solution of the integral form [55] and the explicit exponential conversion method [56]. For the numerical solution, the creep compliance is substituted into Equation (12), and the corresponding relaxation modulus is then calculated. The explicit exponential conversion method, proposed by Li [30] and van Breugel [31], has shown strong accuracy for estimating early-age stress in both PC and AAS/AASF concrete.

4.3.1 Numerical solution

By numerically solving the integral relation Equation (12), the relaxation function $R(t,t')$ can be obtained from the given creep compliance function $J(t,t')$ as follows:

$$R(1,t') = 0 \quad (19)$$

$$R(2,t') = \frac{1}{J(t',t')} \quad (20)$$

$$\begin{aligned}&R(k+1,t') \\ &= R(k,t') - \frac{1}{J_{k,k+1}}\sum_{i=1}^{k-1}\Delta J_{i,k}(R(i+1,t') - R(i,t'))\end{aligned} \quad (21)$$

$$J_{k,k+1} = \frac{J(k+1,k+1)+J(k,k+1)}{2} \quad (22)$$

$$\Delta J_{i,k} = J(k,i+1) - J(k,i) \quad (23)$$

where k is the time step, i.e., from 1 to t.

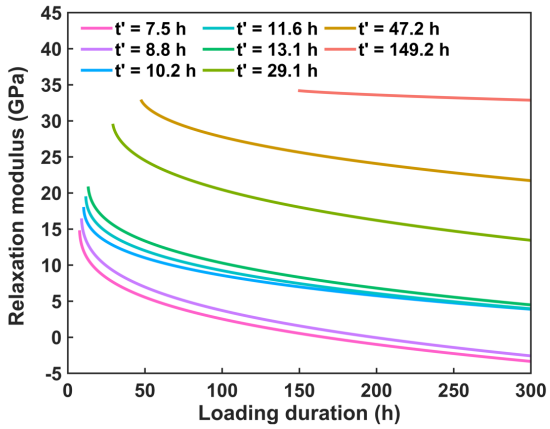

Figure 7. Relaxation modulus calculated by numerical solution.

According to Equations from (19) to (23) to, the results of relaxation modulus calculated by numerical solution are shown in Figure 7. It is obvious that the relaxation modulus values decrease with time, which is consistent with the viscoelastic properties of AASC. However, from 166 h, the relaxation modulus (for example, $t = 7.5h\ or\ t' = 8.1h$)

does not converge to zero but instead to negative values. The results suggest that it may not capture the real stress relaxation over longer durations. This implies that during the relaxation process, stress not only diminishes but also reverses direction, which is an impractical phenomenon. However, a negative relaxation modulus, mathematically, can reflect the dominance of microstructural densification, which lead to rapid increment of E-modulus and can cause the relaxation modulus to appear as though it is decreasing, despite ongoing creep. This could be an argument especially for AASC, where the modulus increases rapidly in the early age. Actually, previous studies (Refs. [43,57]) have noted this issue, attributing it to the high nonlinearity of the relaxation modulus, which often leads to underestimation by numerical solution. The negative relaxation modulus only appears initially and is mainly an issue in very early-age materials with high creep, but is negligible in long-term creep analysis.

4.3.2 The explicit exponential conversion

Based on the linear superposition principle of creep and relaxation, the total strain ε is composed of an elastic part ε_{el} and a creep part: $\varepsilon = \varepsilon_{el} + \varepsilon_c$. In the fully restrained relaxation testing, the total strain is zero:

$$\varepsilon = \varepsilon_{el} + \varepsilon_c = 0 \tag{24}$$

By applying Hooke's Law to express the linear relationship between the elastic strain and stress, i.e. $\sigma = E(t_o)\varepsilon_{el}$, and taking derivative both sides, Equation (24) can be expressed as below:

$$\frac{1}{E(t_0)}\frac{d\sigma}{dt} = -\frac{\varepsilon_c}{dt} \tag{25}$$

Assuming that the creep strain at a particular time t' can be formulated using the double power law function, i.e., $J(t,t') = a(1/t')^b(t-t')^c$, Equation (25) can be reformulated as:

$$\frac{1}{E(t_0)}\frac{d\sigma}{dt} = -\sigma \cdot a(1/t')^b \cdot c(t-t')^{c-1} \tag{26}$$

It should be noted that both a and n are fitting parameters of the creep model. Integrating Equation (26) and taking the initial stress as σ_0, we get:

$$\frac{\sigma}{\sigma_0} = e^{-E(t')\cdot a\cdot(1/t')^b(t-t')^c} \tag{27}$$

Thus, it can be expressed as the form of relaxation modulus:

$$R(t,t') = e^{1-J(t,t')E(t')}E(t') \tag{28}$$

By substituting the experimentally determined elastic modulus and creep compliance into Equation (28), an explicit expression for the relaxation modulus can be obtained, as shown in Figure 8. Note that the exponent in Equation (28) is exactly the negative of the creep coefficient.

Compared to the numerical solution (Figure 7), the explicit exponential conversion method (Figure 8) provides a more intuitive and computationally efficient approach, yielding a reasonable relaxation modulus for virtual relaxation tests [57,58]. This method avoids the iterative calculations required in Equations (19) to (23). Additionally, the relaxation modulus by the explicit exponential conversion method exhibits a more significant decay curve at early stage. As the results of explicit exponential conversion method converge to zero over time, it is expected to provide a more accurate long-term prediction, capturing the material behavior under prolonged strain.

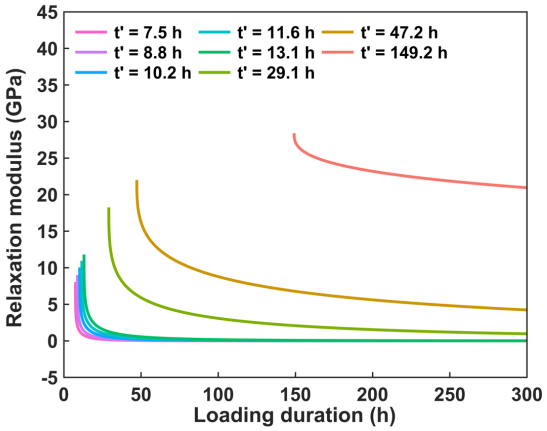

Figure 8. Relaxation modulus calculated by the explicit exponential conversion method.

4.4 Stress prediction

The accurate prediction of internal stress in the AASC during hardening is crucial for understanding its mechanical performance under restrained conditions. As discussed in previous sections, this study employs a viscoelastic framework featuring a double power law to effectively simulate stress evolution based on data from repeated minutes-long creep tests.

Figure 9 compares the predicted internal stress with experimental measurements (For detailed calculation code, see Supplementary information). The explicit exponential method (the red dashed line with an RMSE of 0.123 MPa) accurately captures the general trend of stress development in AASC, demonstrating superior accuracy and closely aligning with the experimental results. The numerical method (the blue dashed line with an RMSE of 0.670 MPa) shows notable deviations relative to the experimental data, especially during the later stages, indicating less accuracy. This supports the conclusion from the previous section that the explicit exponential method not only offers better accuracy but also enhances computational efficiency by avoiding complex iterative procedures. In contrast, the numerical method requires further improvement [55], as issues such as non-physical negative values in the relaxation modulus become increasingly evident over time.

The poor performance of the elastic model, indicated by the highest RMSE, highlights the critical need to incorporate viscoelastic effects. Neglecting these factors results in an incomplete understanding of stress development, especially during early-age periods when the material is most susceptible to cracking [12,59,60]. To accurately capture stress mechanisms, it is essential to consider creep and stress relaxation.

The TSTM system employed by this study accurately models viscoelastic effects, demonstrating reliability for examining

the time-dependent mechanical properties of the AASC. These findings offer valuable insights into early-age stress development in AASC.

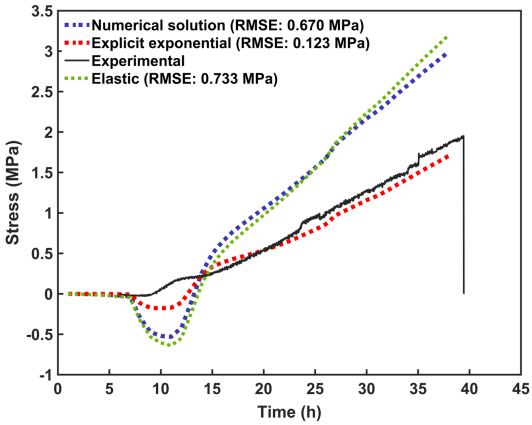

Figure 9. Experimental and numerical results of the internal stress.

5 Conclusions

In this study, the viscoelastic properties of alkali-activated slag (AAS) concrete at early age were systematically investigated through an experimental approach using minutes-long creep tests conducted on a Temperature Stress Testing Machine (TSTM). The findings provide key insights into the time-dependent behavior of AASC, emphasizing the importance of viscoelastic effects, such as creep and stress relaxation, in early-age stress prediction. The following key conclusions can be drawn from this study:

1. The experimental method, which involved repeated minutes-long creep tests, proved effective in quantifying the early-age viscoelastic behavior of AASC during hardening. The TSTM enabled precise measurement of time-dependent creep and stress evolution, providing reliable data for inform predictive models. This method is particularly valuable for studying the rapid viscoelastic changes in the early hydration stages of AASC.
2. The results demonstrate that viscoelastic effects, including creep and stress relaxation, must be considered by models when predict early-age stress development in AASC. Using the double power law function to model creep behavior showed close alignment with experimental data, highlighting its applicability for predicting short-term creep of both unrestrained and restrained AAS materials.
3. Converting creep compliance into a relaxation modulus is critical for simulating the stress relaxation behavior of AASC. This study compared two conversion methods, numerical solution and explicit exponential method, finding that the explicit exponential method provides more accurate long-term predictions. Effectively modelling stress relaxation is crucial for understanding how AASC dissipates stress over time, especially in crack prediction.
4. Future research should investigate the role of temperature fluctuations in viscoelastic behavior, as thermal variation during early hydration can significantly impact stress development. Additionally, further studies should focus on integrating real-world influences such as environmental factors and long-term loading conditions into advanced viscoelastic models to improve the accuracy of stress prediction.

Acknowledgements

Zhenming Li would like to acknowledge the Guangdong Provincial Key Laboratory of Intelligent and Resilient Structures for Civil Engineering (2023B1212010004), Guangdong Basic and Applied Basic Research Foundation (2023A1515111138) and Basic Research Fund in Shenzhen Natural Science Foundation (JCYJ20240813110519025).

Authorship statement (CRediT)

Zhenming Li: Conceptualization, Investigation, Methodology, Validation, Writing – Review & Editing. **Jiawei Xu:** Methodology, Writing – Original Draft, Data Curation, Visualization, Software. **Minfei Liang:** Data curation. **Guang Ye:** Methodology. **Jinping Ou:** Supervision, Writing – Review & Editing.

Appendix A

In addition to the repeated minutes-long creep tests, the test duration was extended. Starting from 28 d, a constant compressive load of 80 kN was applied and maintained for 7 days. Figure A1 compares the creep coefficient after 28 days with the results reported in Ref. [41].

In the study [41], the specimens were demolded 24 h after casting and subsequently subjected to two different curing regimes for 28 days: sealed curing and moist curing. For the sealed curing, the specimens were wrapped in plastic film and stored in a room maintained at 20 ± 2 °C. In the moist curing regime, the specimens were placed in a fog room with 100% relative humidity. Following the 28-day curing period, some specimens remained under their respective curing conditions, while others were transferred to a controlled environment with a temperature of 23 ± 2 °C and a relative humidity of 55 ± 5% to test their creep properties.

The RMSE between the sealed specimen from Ref. [41] and the specimen in this study is 0.1532, while the RMSE for the moist curing specimen is 0.0281. It is generally impossible that the environmental conditions are exactly the same during different experiment. Additionally, systematic and human errors are inevitable. With these constraints, the results of this study can be considered acceptable. As discussed in Ref. [41], the influence of curing conditions on creep properties is linked to microstructure variations. The results confirm the reliability of the repeated minutes-long creep tests on the TSTM in the long term.

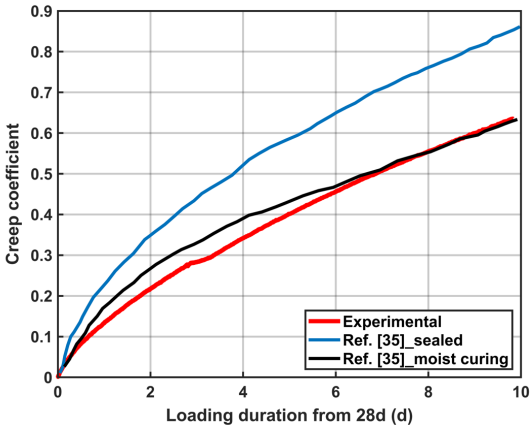

Figure A1. Comparison of creep coefficient from 28 days with Kostiuchenko [41].

References

[1] J.L. Provis, Alkali-activated materials, Cem. Concr. Res. 114 (2018) 40-48. https://doi.org/10.1016/j.cemconres.2017.02.009

[2] C. Shi, B. Qu, J.L. Provis, Recent progress in low-carbon binders, Cem. Concr. Res. 122 (2019) 227-250. https://doi.org/10.1016/j.cemconres.2019.05.009

[3] M.C.G. Juenger, F. Winnefeld, J.L. Provis, J.H. Ideker, Advances in alternative cementitious binders, Cem. Concr. Res. 41 (2011) 1232-1243. https://doi.org/10.1016/j.cemconres.2010.11.012

[4] P. Awoyera, A. Adesina, A critical review on application of alkali activated slag as a sustainable composite binder, Case Stud. Constr. Mater. 11 (2019) e00268. https://doi.org/10.1016/j.cscm.2019.e00268

[5] A. Fernández-Jiménez, J.G. Palomo, F. Puertas, Alkali-activated slag mortars Mechanical strength behaviour, Cem. Concr. Res. 29 (1999) 1313-1321. https://doi.org/10.1016/S0008-8846(99)00154-4

[6] S. Aydın, B. Baradan, Effect of activator type and content on properties of alkali-activated slag mortars, Compos. Part B Eng. 57 (2014) 166-172. https://doi.org/10.1016/j.compositesb.2013.10.001

[7] M. Chi, Effects of dosage of alkali-activated solution and curing conditions on the properties and durability of alkali-activated slag concrete, Constr. Build. Mater. 35 (2012) 240-245. https://doi.org/10.1016/j.conbuildmat.2012.04.005

[8] M. Nedeljković, Z. Li, G. Ye, Setting, Strength, and Autogenous Shrinkage of Alkali-Activated Fly Ash and Slag Pastes: Effect of Slag Content, Materials 11 (2018) 2121. https://doi.org/10.3390/ma11112121

[9] M.A. Longhi, Z. Zhang, B. Walkley, E.D. Rodríguez, A.P. Kirchheim, Strategies for control and mitigation of efflorescence in metakaolin-based geopolymers, Cem. Concr. Res. 144 (2021) 106431. https://doi.org/10.1016/j.cemconres.2021.106431

[10] Z. Li, T. Lu, Y. Chen, B. Wu, G. Ye, Prediction of the autogenous shrinkage and microcracking of alkali-activated slag and fly ash concrete, Cem. Concr. Compos. 117 (2021) 103913. https://doi.org/10.1016/j.cemconcomp.2020.103913

[11] M. Liang, Z. Chang, P. Holthuizen, Y. Chen, S. He, E. Schlangen, B. Šavija, Efficiently assessing the early-age cracking risk of cementitious materials with a mini temperature stress testing machine, Cem. Concr. Compos. 153 (2024) 105710. https://doi.org/10.1016/j.cemconcomp.2024.105710

[12] Z. Li, S. Zhang, X. Liang, G. Ye, Cracking potential of alkali-activated slag and fly ash concrete subjected to restrained autogenous shrinkage, Cem. Concr. Compos. 114 (2020) 103767. https://doi.org/10.1016/j.cemconcomp.2020.103767

[13] Z. Li, Y. Chen, J.L. Provis, Ö. Cizer, G. Ye, Autogenous shrinkage of alkali-activated slag: A critical review, Cem. Concr. Res. 172 (2023) 107244. https://doi.org/10.1016/j.cemconres.2023.107244

[14] H. Ye, A. Radlińska, Shrinkage mechanisms of alkali-activated slag, Cem. Concr. Res. 88 (2016) 126-135. https://doi.org/10.1016/j.cemconres.2016.07.001

[15] Z. Li, X. Liang, Y. Chen, G. Ye, Effect of metakaolin on the autogenous shrinkage of alkali-activated slag-fly ash paste, Constr. Build. Mater. 278 (2021) 122397. https://doi.org/10.1016/j.conbuildmat.2021.122397

[16] S.Y. Abate, S. Park, H.-K. Kim, Parametric modeling of autogenous shrinkage of sodium silicate-activated slag, Constr. Build. Mater. 262 (2020) 120747. https://doi.org/10.1016/j.conbuildmat.2020.120747

[17] M.K. Tadros, A. Ghali, W.H. Dilger, Time-dependent prestress loss and deflection in prestressed concrete members, PCI J. 20 (1975) 86-98. https://doi.org/10.15554/pcij.05011975.86.98

[18] A.E. Naaman, S.-H. Chao, Prestressed concrete analysis and design: Fundamentals, in: McGraw- Hill New York, 1982.

[19] A. Delsaute, J.-M. Torrenti, S. Staquet, Modeling basic creep of concrete since setting time, Cem. Concr. Compos. 83 (2017) 239-250. https://doi.org/10.1016/j.cemconcomp.2017.07.023

[20] M. Serdar, I. Gabrijel, D. Schlicke, S. Staquet, M. Azenha, eds., Advanced Techniques for Testing of Cement-Based Materials, Springer International Publishing, Cham, 2020. https://doi.org/10.1007/978-3-030-39738-8

[21] A. Delsaute, J.-M. Torrenti, S. Staquet, Modeling basic creep of concrete since setting time, Cem. Concr. Compos. 83 (2017) 239-250. https://doi.org/10.1016/j.cemconcomp.2017.07.023

[22] B. Delsaute, C. Boulay, S. Staquet, Creep testing of concrete since setting time by means of permanent and repeated minute-long loadings, Cem. Concr. Compos. 73 (2016) 75-88. https://doi.org/10.1016/j.cemconcomp.2016.07.005

[23] Z.P. Bažant, E. Osman, Double power law for basic creep of concrete, Matér. Constr. 9 (1976) 3-11. https://doi.org/10.1007/BF02478522

[24] C.A. Jones, Z.C. Grasley, Short-term creep of cement paste during nanoindentation, Cem. Concr. Compos. 33 (2011) 12-18. https://doi.org/10.1016/j.cemconcomp.2010.09.016

[25] M. Vandamme, F.-J. Ulm, Nanoindentation investigation of creep properties of calcium silicate hydrates, Cem. Concr. Res. 52 (2013) 38-52. https://doi.org/10.1016/j.cemconres.2013.05.006

[26] M. Irfan-ul-Hassan, M. Königsberger, R. Reihsner, C. Hellmich, B. Pichler, How Water-Aggregate Interactions Affect Concrete Creep: Multiscale Analysis, J. Nanomechanics Micromechanics 7 (2017) 04017019. https://doi.org/10.1061/(ASCE)NM.2153-5477.0000135

[27] Z. Chen, H. Wang, J. Zhuo, C. You, Experimental and numerical study on effects of deflectors on flow field distribution and desulfurization efficiency in spray towers, Fuel Process. Technol. 162 (2017) 1-12. https://doi.org/10.1016/j.fuproc.2017.03.024

[28] A. Binder, M. Koenigsberger, R.D. Flores, H.A. Mang, C. Hellmich, B.L.A. Pichler, Thermally activated viscoelasticity of cement paste: Minute-long creep tests and micromechanical link to molecular properties, Cem. Concr. Res. 163 (2023). https://doi.org/10.1016/j.cemconres.2022.107014

[29] A. Naqi, B. Delsaute, M. Konigsberger, S. Staquet, Monitoring early age elastic and viscoelastic properties of alkali-activated slag mortar by means of repeated minute-long loadings, Dev. BUILT Environ. 16 (2023). https://doi.org/10.1016/j.dibe.2023.100275

[30] Z. Li, T. Lu, X. Liang, H. Dong, G. Ye, Mechanisms of autogenous shrinkage of alkali-activated slag and fly ash pastes, Cem. Concr. Res. 135 (2020) 106107. https://doi.org/10.1016/j.cemconres.2020.106107

[31] K. Van Breugel, Relaxation of young concrete, Rep. Stevin Lab. Concr. Struct. 5-80-D8 (1980). https://resolver.tudelft.nl/uuid:da1c2e2e-1cef-4583-9deb-9e1c1f548df9.

[32] C. Boulay, M. Crespini, B. Delsaute, S. Staquet, Monitoring of the creep and the relaxation behaviour of concrete since setting time, part 1: compression, in: Strateg. Sustain. Concr. Struct., 2012: p. 10p.

[33] B. Delsaute, C. Boulay, S. Staquet, Creep testing of concrete since setting time by means of permanent and repeated minute-long loadings, Cem. Concr. Compos. 73 (2016) 75-88.

https://doi.org/10.1016/j.cemconcomp.2016.07.005
[34] Z. Li, X. Liang, C. Liu, M. Liang, K. Van Breugel, G. Ye, Thermal deformation and stress of alkali-activated slag concrete under semi-adiabatic condition: Experiments and simulations, Cem. Concr. Res. 159 (2022) 106887. https://doi.org/10.1016/j.cemconres.2022.106887
[35] S.J. Lokhorst, Deformational behaviour of concrete influenced by hydration related changes of the microstructure, Delft University of technology, 2001.
[36] O. Bernard, F.-J. Ulm, J.T. Germaine, Volume and deviator creep of calcium-leached cement-based materials, Cem. Concr. Res. 33 (2003) 1127-1136. https://doi.org/10.1016/S0008-8846(03)00021-8
[37] M. Irfan-ul-Hassan, B. Pichler, R. Reihsner, Ch. Hellmich, Elastic and creep properties of young cement paste, as determined from hourly repeated minute-long quasi-static tests, Cem. Concr. Res. 82 (2016) 36-49. https://doi.org/10.1016/j.cemconres.2015.11.007
[38] M. Fernández Ruiz, A. Muttoni, P.G. Gambarova, Relationship between Nonlinear Creep and Cracking of Concrete under Uniaxial Compression, J. Adv. Concr. Technol. 5 (2007) 383-393. https://doi.org/10.3151/jact.5.383
[39] C. Videla, D.J. Carreira, N. Garner, Guide for modeling and calculating shrinkage and creep in hardened concrete, ACI Rep. 209 (2008) 76.
[40] M. Liang, Z. Li, S. He, Z. Chang, Y. Gan, E. Schlangen, B. Šavija, Stress evolution in restrained GGBFS concrete due to autogenous deformation: bayesian optimization of aging creep, Constr. Build. Mater. 324 (2022) 126690. https://doi.org/10.1016/j.conbuildmat.2022.126690
[41] A. Kostiuchenko, Creep of alkali-activated slag and fly ash concrete unveiling multiscale dynamics, Delft University of Technology, 2023.
[42] Z.P. Bažant, S.T. Wu, Rate-type creep law of aging concrete based on maxwell chain, Matér. Constr. 7 (1974) 45-60. https://doi.org/10.1007/BF02482679
[43] Z.P. Bažant, M. Jirásek, Creep and Hygrothermal Effects in Concrete Structures, Springer Netherlands, Dordrecht, 2018. https://doi.org/10.1007/978-94-024-1138-6
[44] B.T. Tamtsia, J.J. Beaudoin, J. Marchand, The early age short-term creep of hardening cement paste: load-induced hydration effects, Cem. Concr. Compos. 26 (2004) 481-489. https://doi.org/10.1016/S0958-9465(03)00079-9
[45] Y. Gan, M. Vandamme, H. Zhang, Y. Chen, E. Schlangen, K. Van Breugel, B. Šavija, Micro-cantilever testing on the short-term creep behaviour of cement paste at micro-scale, Cem. Concr. Res. 134 (2020) 106105. https://doi.org/10.1016/j.cemconres.2020.106105
[46] R. De Borst, A.H. Van den Boogaard, Finite‐Element Modeling of Deformation and Cracking in Early‐Age Concrete, J. Eng. Mech. 120 (1994) 2519-2534. https://doi.org/10.1061/(ASCE)0733-9399(1994)120:12(2519). https://doi.org/10.1061/(ASCE)0733-9399(1994)120:12(2519)
[47] B. Delsaute, S. Staquet, Early age creep and relaxation modelling of concrete under tension and compression, in: Proc. RILEM Int. Symp. Concr. Model., CONMOD, 2014: pp. 168-175.
[48] J. Baronet, L. Sorelli, J.-P. Charron, M. Vandamme, J. Sanahuja, A two-scale method to rapidly characterize the logarithmic basic creep of concrete by coupling microindentation and uniaxial compression creep test, Cem. Concr. Compos. 125 (2022) 104274. https://doi.org/10.1016/j.cemconcomp.2021.104274
[49] F.H. Wittmann, J. Lukas, The application of rate theory to time-dependent deformation of concrete, Mag. Concr. Res. 26 (1974) 191-197. https://doi.org/10.1680/macr.1974.26.89.191
[50] P. Rossi, J.L. Tailhan, F. Le Maou, Creep strain versus residual strain of a concrete loaded under various levels of compressive stress, Cem. Concr. Res. 51 (2013) 32-37. https://doi.org/10.1016/j.cemconres.2013.04.005
[51] L. Su, Y. Wang, S. Mei, P. Li, Experimental investigation on the fundamental behavior of concrete creep, Constr. Build. Mater. 152 (2017) 250-258. https://doi.org/10.1016/j.conbuildmat.2017.06.162
[52] B.T. Tamtsia, J.J. Beaudoin, Basic creep of hardened cement paste A re-examination of the role of water, Cem. Concr. Res. 30 (2000) 1465-1475. https://doi.org/10.1016/S0008-8846(00)00279-9
[53] B.T. Tamtsia, J.J. Beaudoin, J. Marchand, The early age short-term creep of hardening cement paste: load-induced hydration effects, Cem. Concr. Compos. 26 (2004) 481-489. https://doi.org/10.1016/S0958-9465(03)00079-9
[54] Z. Hu, A. Hilaire, J. Ston, M. Wyrzykowski, P. Lura, K. Scrivener, Intrinsic viscoelasticity of C-S-H assessed from basic creep of cement pastes, Cem. Concr. Res. 121 (2019) 11-20. https://doi.org/10.1016/j.cemconres.2019.04.003
[55] Z.P. Bažant, M. Jirásek, Creep and Hygrothermal Effects in Concrete Structures, Springer Netherlands, Dordrecht, 2018. https://doi.org/10.1007/978-94-024-1138-6
[56] K. Van Breugel, Relaxation of young concrete, Rep. Stevin Lab. Concr. Struct. 5-80-D8 (1980).
[57] M. Liang, G.D. Luzio, E. Schlangen, B. Šavija, Experimentally informed modeling of the early‐age stress evolution in cementitious materials using exponential conversion from creep to relaxation, Comput.-Aided Civ. Infrastruct. Eng. (2024) mice.13156. https://doi.org/10.1111/mice.13156
[58] M. Liang, J. Xie, S. He, Y. Chen, E. Schlangen, B. Šavija, Autogenous deformation-induced stress evolution in cementitious materials considering viscoelastic properties: A review of experiments and models, Dev. Built Environ. 17 (2024) 100356. https://doi.org/10.1016/j.dibe.2024.100356
[59] M. Azenha, F. Kanavaris, D. Schlicke, A. Jędrzejewska, F. Benboudjema, T. Honorio, V. Šmilauer, C. Serra, J. Forth, K. Riding, B. Khadka, C. Sousa, M. Briffaut, L. Lacarrière, E. Koenders, T. Kanstad, A. Klausen, J.-M. Torrenti, E.M.R. Fairbairn, Recommendations of RILEM TC 287-CCS: thermo-chemo-mechanical modelling of massive concrete structures towards cracking risk assessment, Mater. Struct. 54 (2021) 135. https://doi.org/10.1617/s11527-021-01732-8
[60] M. Liang, Y. Gan, C. Ze, W. Zhi, E. Schlangen, B. Šavija, Microstructure-informed deep convolutional neural network for predicting short-term creep modulus of cement paste, Cem. Concr. Res. 152 (2022) 106681. https://doi.org/10.1016/j.cemconres.2021.106681